Electronic Supplementary Information

Cu nanoclusters loaded N-doped porous graphitic carbons for electrochemical CO2 reduction towards syngas generation

Xuefu Hu,[#a] Haiyue Lu,[#a] Gen Li,[a] Baicheng Liao,[a] Xiuli Zhang,[a] and Liyong Chen,*[a,b]

[a]Department of Pharmaceutical Engineering, Bengbu Medical College, Bengbu, 233030, China. E-mail: lychen@bbmc.edu.cn; huxuefu@bbmc.edu.cn.
[b]Anhui Province Key Laboratory of Translational Cancer Research, Bengbu Medical College, Bengbu, 233030, China.

Experimental Section

Materials and characterization methods

All chemical reagents were used as received. Nafion solution (5 wt% in mixture of water and 2-propanol) was purchased from Sigma Aldrich, and other chemicals and solvents, including zinc nitrate ($Zn(NO_3)_2 \cdot 6H_2O$), copper(II) nitrate ($Cu(NO_3)_2 \cdot 3H_2O$), 2-methylimidazole (Hmim), methanol (MeOH), ethanol (EtOH), and potassium bicarbonate ($KHCO_3$), were purchased from Sinopharm Chemical Reagent Co., Ltd, China.

Scanning electron microscopy (SEM) and transmission electron microscopy (TEM) were performed for microstructural and morphological characterization on HITACHI UHR FE-SEM SU8220 and Talos F200S-G2, respectively. High-angle annular dark field-scanning transmission electron microscopy (HAADF-STEM) was carried out on Grand ARMF2. X-ray diffraction (XRD) was conducted in a Rigaku D/Max 2400 automatic powder X-ray diffractometer with Cu-Kα radiation (λ = 1.5418 Å). Linear-sweep voltammetry (LSV), cyclic voltammetry (CV), and electrochemical impedance spectroscopy (EIS) were carried out using a CHI760E electrochemical workstation with a typical three-electrode H-type cell. N_2 sorption isotherm at 77 K and CO_2 uptake at 293 K were obtained using a Micromeritics 3Flex surface characterization analyzer and Micromeritics TriStar II Plus automatic surface characterization analyzer, respectively. The content of Cu was evaluated by inductively coupled plasma atomic emission spectroscopy (ICP-AES) on Optima 2000DV. Gas chromatograph (GC7900 Techcomp) was performed on analyzing the gas products. 1H NMR analysis was conducted with a Bruker AC-400FT spectrometer (400 MHz) to analyze the liquid products.

Materials synthesis

Synthesis of Cu-doped ZIF-8

Solution A: 2-methylimidazole (Hmim, 3.3g, 8mmol) in 60 mL of MeOH;

Solution B: $Zn(NO_3)_2 \cdot 6H_2O$ (1.339 g, 0.9 mmol) and $Cu(NO_3)_2 \cdot 3H_2O$ (0.121 g, 0.1 mmol) in 60 mL of MeOH.

Solution A was added dropwise to solution B with continuous stirring. The resulting mixture was stirred for an additional hour at room temperature, and the final product (Cu-doped ZIF-8) was collected by centrifugation, washed three times with ethanol, and dried overnight under ambient conditions.

Synthesis of Cu nanoclusters loaded N-doped porous graphitic carbons_10 (Cu/N-pg-C_10)

The as-made Cu-doped ZIF-8 (~100 mg) was loaded onto a porcelain boat and annealed at 1000 °C in a tubular furnace ramping at 2 °C/min in a 5% H_2/Ar atmosphere and maintained at temperature for 2 h.

To prepare different Cu nanoclusters loaded N-doped porous graphitic carbon (Cu/N-*pg*-C_5 and Cu/N-*pg*-C_20), solution A can be adjusted by the choice of $Zn(NO_3)_2 \cdot 6H_2O$ and $Cu(NO_3)_2 \cdot 3H_2O$ with different amount in MeOH. For example, the molar ratio of Cu^{2+} to total metal ions was 1:20 (5%) and 1:5 (20%), where the total mole of metal ions was 1 mmol.

Synthesis of N-doped porous graphitic carbons (N-pg-C)

The solution of Hmim (3.3g) in MeOH (60 mL) was added to the solution of $Zn(NO_3)_2 \cdot 6H_2O$ (1.488 g) in MeOH (60 mL) with continuous stirring. The resulting mixture was stirred for an additional hour at room temperature, and the final product (ZIF-8) was collected by centrifugation, washed three times with ethanol, and dried overnight under ambient conditions.

ZIF-8 (~100 mg) was loaded onto a porcelain boat and annealed at 1000 °C in a tubular furnace ramping at 2 °C/min in a 5% H_2/Ar atmosphere and maintained at temperature for 2 h.

Electrochemical measurements

The performance of the as-made electrocatalysts in CO_2RR was assessed using a gas-tight H-type cell separated by an ion-exchange membrane (Nafion 117) at CHI 760E electrochemical workstation. The electrolyte was Ar- or CO_2-saturated 0.5 M $KHCO_3$ solution. Ag/AgCl (saturated KCl solution), polished Pt wire, and self-supported electrocatalysts (1 × 1 cm^2) were used as reference electrode, counter electrode, and working electrode, respectively. The measured potentials were converted to the

corresponding potentials of the reversible hydrogen electrode using the equation, $E_{RHE} = E_{Ag/AgCl} + 0.197\ V + 0.0591 \times pH$. Electrochemical impedance spectrums (EIS) were collected with frequencies from 0.1 Hz to 100 kHz. LSV tests were performed in Ar- or CO_2-saturated 0.5 M $KHCO_3$ solution at a sweep rate of 5 mV s^{-1} between -1.0 V and 0 V vs RHE. CV tests were carried out in CO_2-saturated 0.5 M $KHCO_3$ solution at variable sweep rate from 10 to 50 mV s^{-1} with an increment of 10 mV s^{-1} between 0.2 V and 0.55 V vs RHE. The long-term stability of the electrocatalysts was estimated via the amperometric *i-t* tests.

Faradaic efficiency (FE) of the products was calculated from the equation, $FE(\%) = \frac{z \times n \times F}{Q} \times 100\%$, wherein z is the number of electrons for generation of product (1 mol), n is the molar amount of the product, F is the Faraday constant of 96485 C mol^{-1}, and Q is the total charge in the electrochemical CO_2RR.

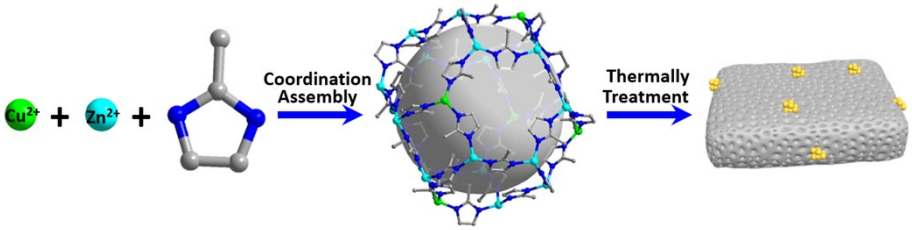

Scheme S1. Schematic illustration of the preparation of Cu nanoclusters loaded N-doped porous graphitic carbons by Cu-doped ZIF-8.

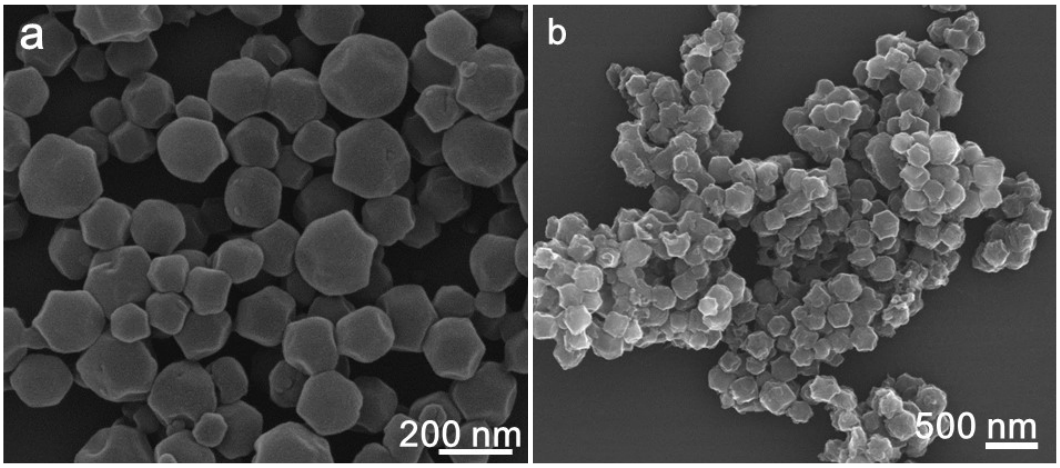

Figure S1. SEM images of (a) Cu-doped ZIF-8 and (b) pure ZIF-8.

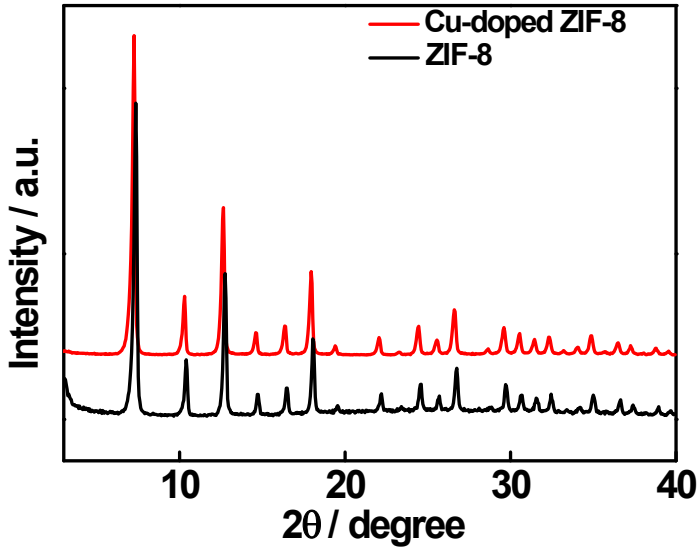

Figure S2. XRD patterns of (a) ZIF-8 and (b) Cu-doped ZIF-8.

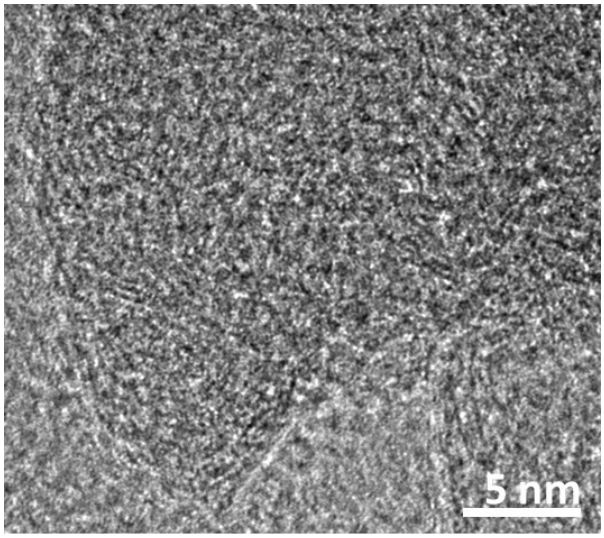

Figure S3. HRTEM image of Cu/N-*pg*-C_10 with graphitic structures.

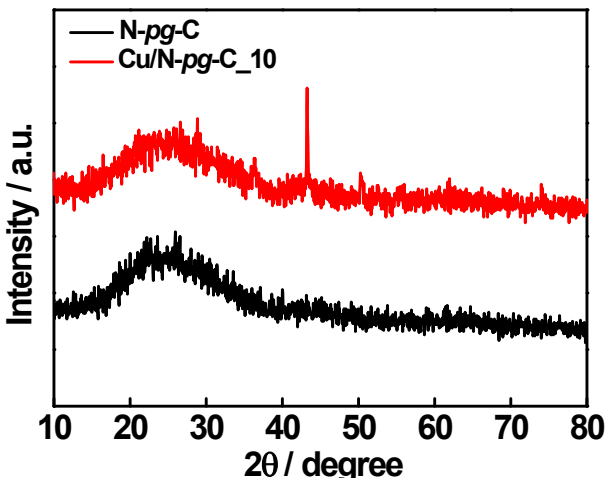

Figure S4. XRD patterns of N-*pg*-C and Cu/N-*pg*-C_10.

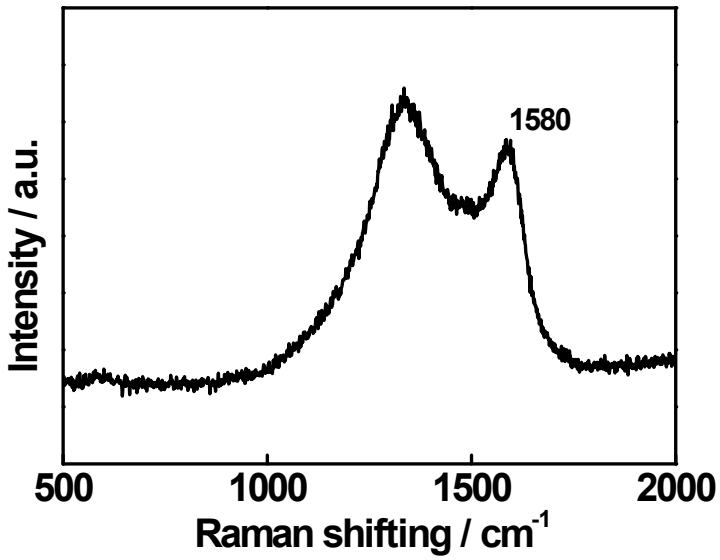

Figure S5. Raman spectrum of Cu/N-*pg*-C_10.

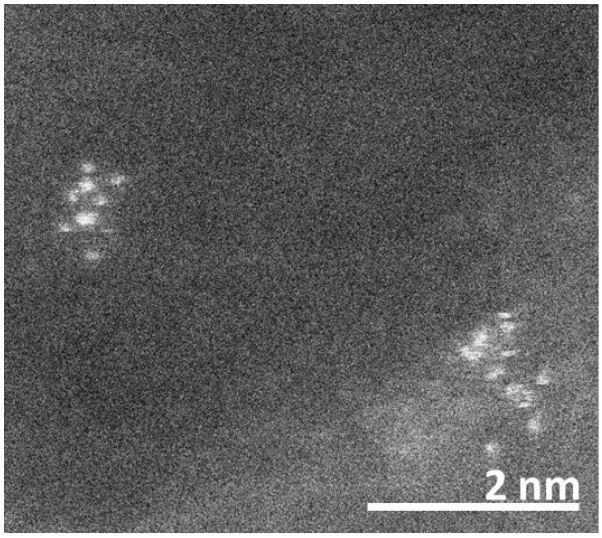

Figure S6. The high-magnified HAADF-STEM image of Cu/N-*pg*-C_10.

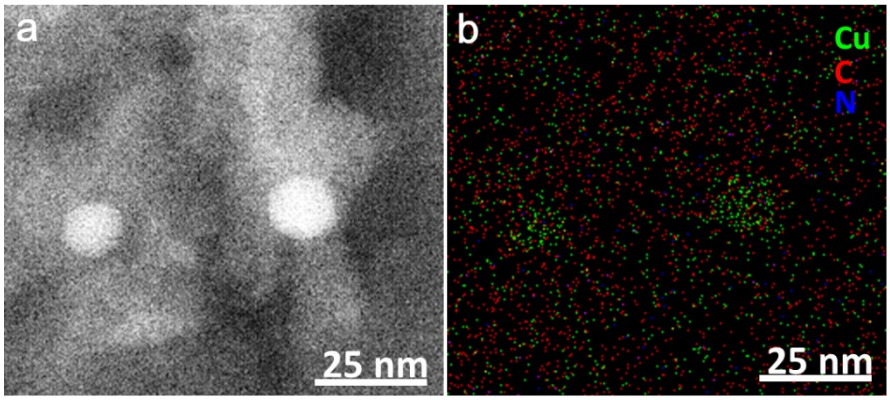

Figure S7. (a) HAADF image of (b) elemental mappings of Cu/N-*pg*-C_10.

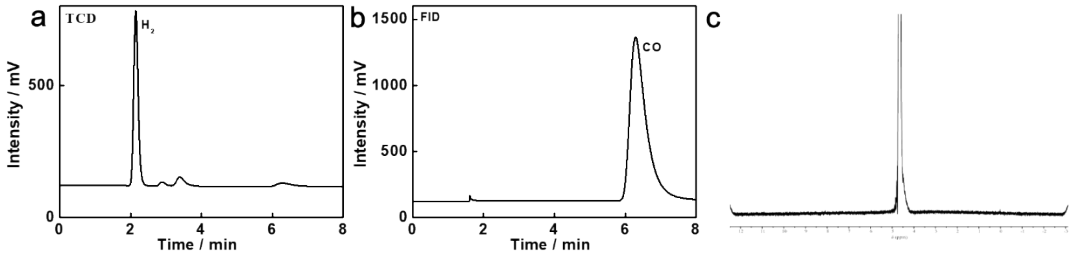

Figure S8. (a, b) GC of gas products and (c) ^{1}H-NMR of liquid products over the Cu/N-*pg*-C_10 electrocatalyst in CO_2-saturated $KHCO_3$ at an applied potential of -0.5 V vs RHE for 1 h.

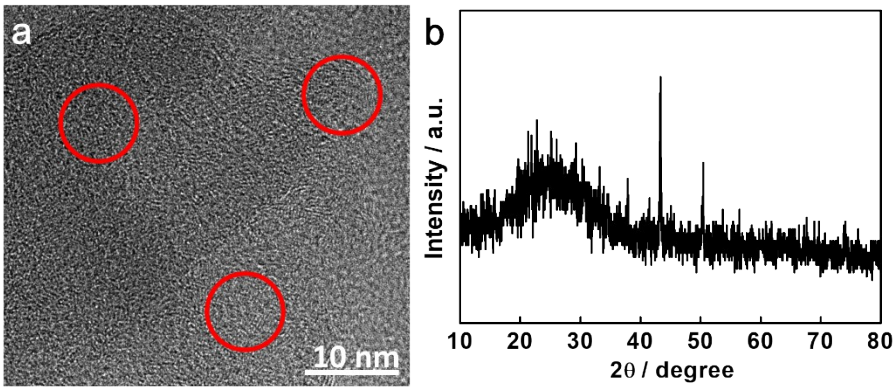

Figure S9. (a) HRTEM image and (b) XRD pattern of Cu/N-*pg*-C_10 after test for stability for 8 h.

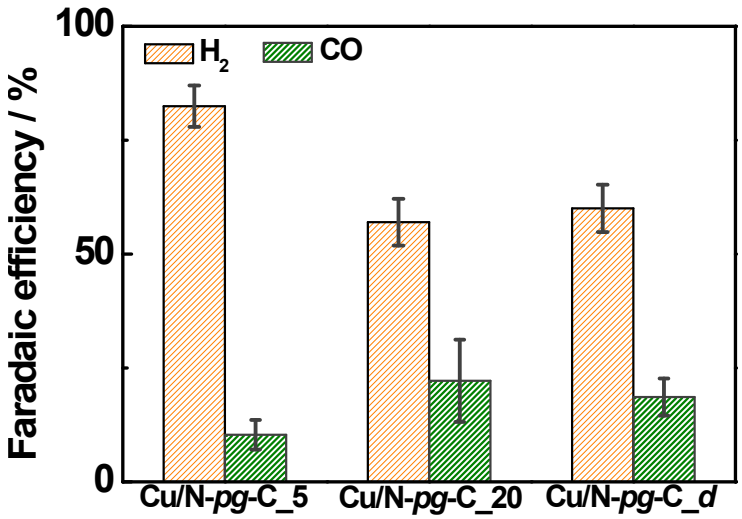

Figure S10. FE_{CO} and FE_{H2} of various electrocatalysts in CO_2-saturated 0.5 M $KHCO_3$ solution at -0.5 V vs RHE.

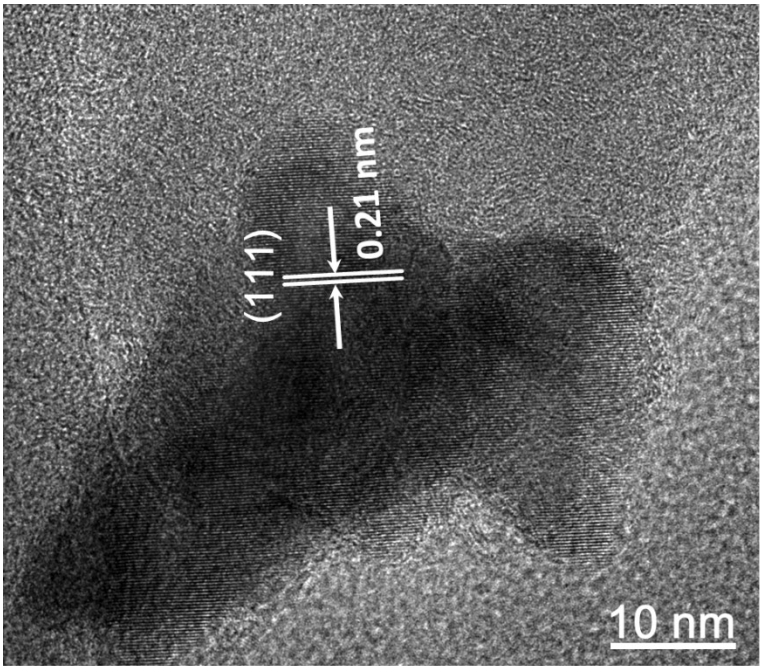

Figure S11. HRTEM image of Cu/N-*pg*-C_20.

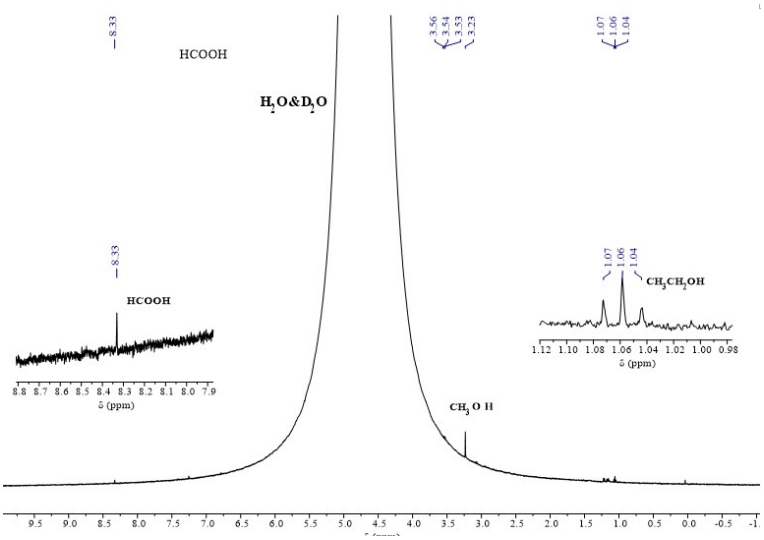

Figure S12. ^{1}H NMR of liquid products over the Cu/N-*pg*-C_20 electrocatalyst in CO_2-saturated $KHCO_3$ at an applied potential of -0.5 V vs RHE for 1 h

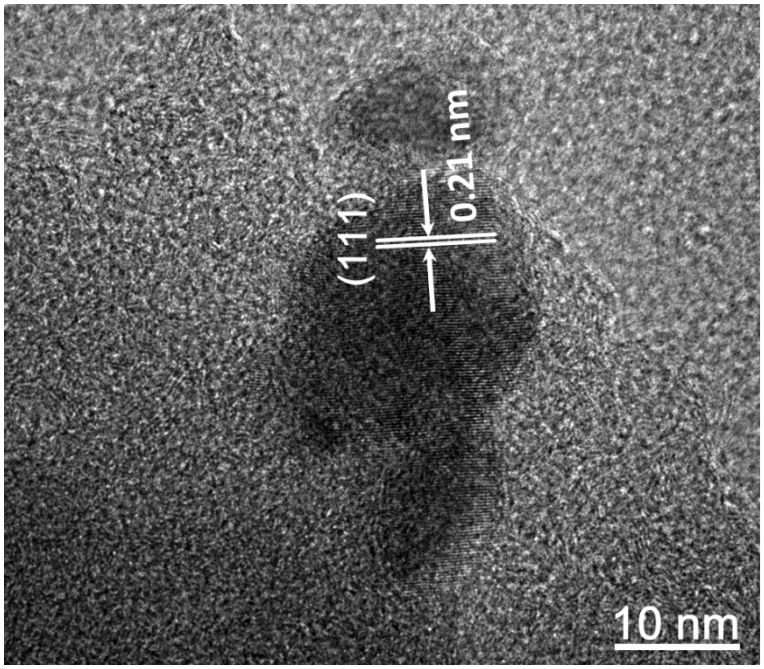

Figure S13. HRTEM image of Cu/N-*pg*-C_*d*.

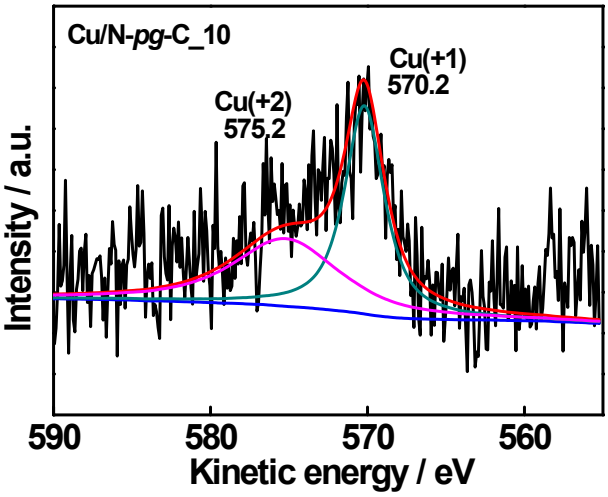

Figure S14. Cu LMM Auger spectrum of Cu/N-pg-C_10.

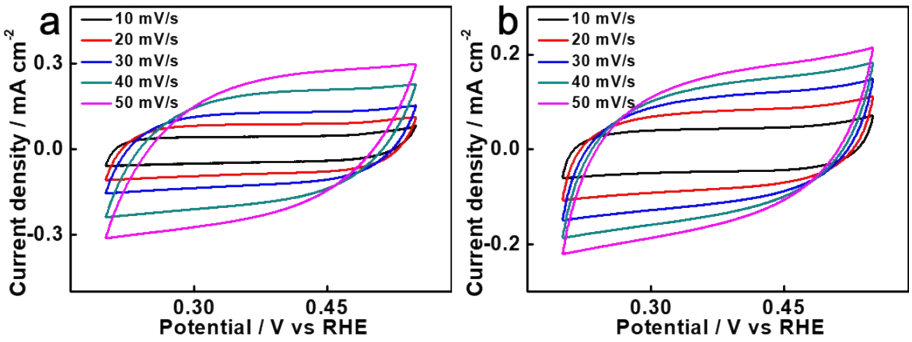

Figure S15. CV curves within a non-faradaic region at different scan rates: (a) Cu/N-*pg*-C_10 and (b) N-*pg*-C

Table S1. Summary of CO_2 electroreduction to syngas using different catalysts.

Catalyst	Electrolyte	Potential （V vs RHE）		Ref
		j_{CO} (mA/cm^{-2})	$R_{H2/CO}$ or FE_{CO}	
Pd/TaC	0.5M $KHCO_3$.	35.9@-0.7; 42.4@-0.8	1:0.6; 1:0.29	1
$Au_{75}Cu_{25}$/C	0.1M $KHCO_3$	28.5@-0.7	92.6%	2
Pd Icosahedra/C	0.1M $KHCO_3$	2.52@-0.7; 4.58@-0.8	1:7.3; 1:11.5	3
oxide-derived Au	0.5M $NaHCO_3$	0.3−0.5@-0.25	~1:1.85	4
Cu_3Se_2-CF	0.1M $KHCO_3$	11.9@-1.2	~1:0.75	5
Cu/In	0.1M $KHCO_3$	~6.5@-0.8; ~8.7@-1.1	1:9; 1:3	6
PdCuCo	0.5M [Bmim]PF_6, 0.5M H_2SO_4	~17@-1.16; ~27.7@-1.36	~1:7; 0.6:1	7
$AuCu_2$/CNT	0.5M $KHCO_3$	3.4@-0.4	95.2%	8
OD-Cu NAs	0.1M $KHCO_3$	1.64@-0.5	1:1.7	9
Cu/In_2O_3 NPs/C-H_2	0.1M $KHCO_3$	~8.5@-0.9	2:1	10
F-Cu_2O/ZIF-8	0.1M $KHCO_3$	NA@-0.7; NA@-0.8	~2:1; 1:3	11
Cu/N-*pg*-C_10	0.5M $KHCO_3$	12.1@-0.5; 7.57@-0.6	~1:3; 1:0.6	this work

Reference

1 J. Wang, S. Kattel, C. J. Hawxhurst, J. H. Lee, B. M. Tackett, K. Chang, N. Rui, C. J. Liu and J. G. Chen, *Angew. Chem. Int. Ed.*, 2019, **58**, 6271-6275.

2 F. Chang, C. Wang, X. Wu, Y. Liu, J. Wei, Z. Bai and L. Yang, *Materials*, 2022, **15**, 5064.

3 W. Zhu, S. Kattel, F. Jiao and J. G. Chen, *Adv. Energy Mater.*, 2019, **9**.

4 Y. Chen, C. W. Li and M. W. Kanan, *J. Am. Chem. Soc.*, 2012, **134**, 19969-19972.

5 Y. Hao, Y. Sun, H. Wang, J. Xue, J. Ren, A. A. S. Devi, M. Y. Maximov, F. Hu and S. Peng, *Electrochim. Acta*, 2023, **449**, 142213.

6 S. A. Mahyoub, F. A. Qaraah, S. Yan, A. Hezam, C. Chen, J. Zhong and Z. Cheng, *J. CO_2 Util.*, 2022, **61**, 102033.

7 S. Yang, P. Zhan, Z. Si, G. Li, M. Chu, C. Liu, L. Lu and P. Qin, *ChemNanoMat*, 2022, **9**, e202200470.

8 H. Chen, Z. Li, Z. Zhang, K. Jie, J. Li, H. Li, S. Mao, D. Wang, X. Lu and J. Fu, *Ind. Eng. Chem. Res.*, 2019, **58**, 15425-15431.

9 Y. Wang, C. Niu, Y. Zhu, D. He and W. Huang, *ACS Appl. Mater. Interfaces*, 2020, **3**, 9841-9847.

10 J. Shen, L. Wang, X. He, S. Wang, J. Chen, J. Wang and H. Jin, *ChemSusChem*, 2022, **15**, e202201350.

11 H. Luo, B. Li, J. G. Ma and P. Cheng, *Angew. Chem. Int. Ed.*, 2022, **61**, e202116736.